ACS OMEGA

http://pubs.acs.org/journal/acsodf

Article

# Computational Analysis of the Mechanism of Nonenzymatic Peptide Bond Cleavage at the C-Terminal Side of an Asparagine Residue

Koichi Kato,* Tomoki Nakayoshi, Yoshinobu Ishikawa, Eiji Kurimoto, and Akifumi Oda

Cite This: *ACS Omega* 2021, 6, 30078−30084

Read Online

ACCESS | Metrics & More | Article Recommendations | Supporting Information

**ABSTRACT:** The nonenzymatic peptide bond cleavage at the C-terminal side of Asn residues is a protein post-translational modification that occurs under physiological conditions. This reaction proceeds much slower than the deamidation of the Asn side chain and causes denaturation and hypofunction of proteins. The peptide bond cleavage of Asn is detected primarily in crystallins and aquaporin 0 in the eye lens. Therefore, cleavage is thought to be involved in age-related cataracts. In this study, to clarify the mechanism underlying succinimide formation for the peptide bond cleavage of the Asn residue, we performed quantum chemical calculations on the model compound Ace-Asn-Gly-Nme (Ace = acetyl and Nme = methylamino). The density functional theory with the B3LYP/6-31+G(d,p) level of theory was used to obtain optimized geometries. The results suggested that the reaction proceeds through two steps, cyclization and C-terminal fragment release, and the required proton transfers can be mediated by $H_2PO_4^-$ and $HCO_3^-$ ions. The conformational change of the main chain on the N-terminal side of Asn was needed for the C-terminal fragmentation step, and a separate conformational change at the C-terminal side was required for the cyclization step. Furthermore, the calculated activation barriers of the reactions catalyzed by the $H_2PO_4^-$ ion (130 kJ $mol^{-1}$) and the $HCO_3^-$ ion (123 kJ $mol^{-1}$) were sufficiently low for the reactions to occur under normal physiological conditions.

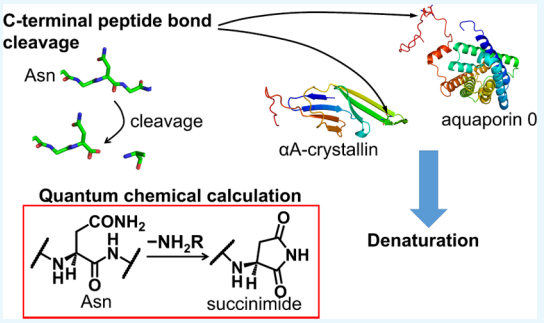


## INTRODUCTION

For Asn residues, two types of nonenzymatic reactions, deamidation of the side chain and peptide bond cleavage of the main chain, have been reported.[1−3] Although deamidation of the Asn side chain is a well-known reaction, peptide bond cleavage of the Asn main chain does not frequently occur. Both reactions of Asn residues are protein post-translational modifications occurring nonenzymatically under physiological conditions. However, those reaction pathways are considered to be different from each other. When the reaction is started by the nucleophilic attack of the main-chain nitrogen at the C-terminal side to the side-chain amide carbon of Asn, the neutral side chain of Asn is transformed into a carboxylic acid, forming an Asp residue or the biologically uncommon isoAsp residues (Figure 1). On the other hand, peptide bond cleavage occurs by the nucleophilic attack of the side-chain nitrogen of Asn to the main-chain amide carbon of Asn. This reaction results in denaturation and hypofunction of the proteins involved and, consequently, causes age-related diseases. In particular, the peptide bond cleavage at the C-terminal side of Asn is reported in αA-crystallin[4] and aquaporin 0 (AQP0)[5] in the eye lens, which are long-lived proteins. The nonenzymatic post-translational modifications trigger the aggregation of lens crystallin.[6,7] AQP0 has essential roles in the maintenance of lens transparency and homeostasis.[8] Moreover, nonenzymatic peptide bond cleavage leads to protein−protein crosslinks.[9] The reaction between Lys and succinimide intermediates results in the crosslinking of AQP0.[10] The AQP0-AQP0 crosslinked peptide is increased in cataract-containing lenses. Therefore, the peptide bond cleavage of Asn is thought to be related to the pathogenesis of cataracts. The protein−protein crosslinking following peptide bond cleavage is required for the maturation of jack bean concanavalin A.[11] This maturation of concanavalin A proceeds slowly due to the rate of peptide bond cleavage of Asn. Furthermore, the fragmentation of monoclonal antibodies has been reported by nonenzymatic peptide bond cleavage.[12,13] The cleavage of monoclonal antibodies is observed in the complementarity-determining and hinge regions and can occur during the purification process, storage, or while circulating in blood. Fragmentation of these regions affects the binding affinity for targets and has an effect on antibody potency. A better understanding of the reaction mechanism would prove useful for the development of the fragmentation-controlling methods. Therefore, the peptide bond cleavage in Asn has important roles in biological and physiological studies.

**Received:** September 1, 2021
**Accepted:** October 14, 2021
**Published:** October 26, 2021

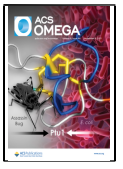

ACS Publications

© 2021 The Authors. Published by American Chemical Society



https://doi.org/10.1021/acsomega.1c04821
*ACS Omega* 2021, 6, 30078−30084

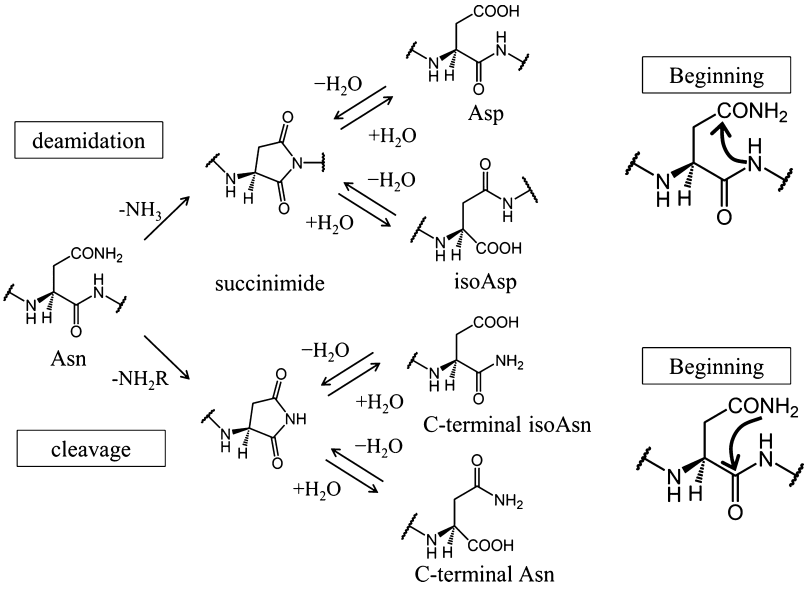


**Figure 1.** Reaction pathway and reaction beginning of deamidation of main-chain and peptide bond cleavage at the C-terminal side of the Asn residue.

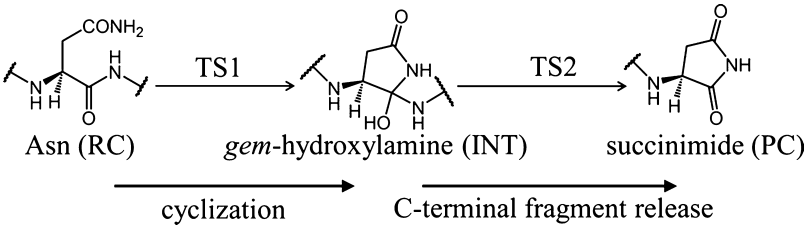


**Figure 2.** Two-step succinimide formation pathway for peptide bond cleavage at the C-terminal side of Asn residues.

Deamidation of side chains in Asn has been suggested to proceed through the cyclic succinimide intermediate at neutral pH.[2] The imide intermediate is formed via the tetrahedral intermediate including the *gem*-hydroxylamine produced by the nucleophilic attack of the main-chain nitrogen of the $(N + 1)$ residue to the amide carbon of the Asn side chain. The peptide bond cleavage of Asn is thought to proceed through the cyclic imide intermediate similar to deamidation. The initial step of peptide bond cleavage is the nucleophilic attack of the side-chain nitrogen of Asn to the main-chain amide carbon of the Asn residue (Figure 1).[2,3] For this reaction pathway, the Asn residue converts to a C-terminal Asn or isoAsn. Although the cleavage and deamidation have similar reaction pathways, the cleavage rate is much slower than the deamidation rate.[14] Robinson and Robinson have previously reported that the Asn peptide deamidation half-times range from about 1 to 400 days, and the Asn cleavage rates range from about 200 to more than 10,000 days at 37 °C.[2] Due to the slow speed of the reaction, the kinetics and the reaction mechanism underlying the peptide bond cleavage of Asn are not well known. In addition, there are no common structural features at the sites of peptide bond cleavage occurring in αA-crystallin and AQP0. Nonenzymatic post-translational modification of proteins generally occurs in regions of high flexibility in the protein, such as intrinsically disordered regions. In AQP0, peptide bond cleavage occurs at Asn246 located within the flexible C-terminal region.[5] However, the reaction proceeds at Asn101 located on the β sheet in αA-crystallin.[4] Therefore, flexibility is not considered to be important for the peptide bond cleavage of Asn. To clarify the effects of the protein structures on the reaction rate for peptide bond cleavage of Asn, we analyzed the reaction mechanism in detail.

In a previous study, water-molecule-catalyzed succinimide formation for peptide bond cleavage of Asn was computationally analyzed.[15] However, the water-catalyzed reaction is not considered to occur under normal physiological conditions because the calculated activation energy is approximately 47.6 kcal $mol^{-1}$ (199 kJ $mol^{-1}$). Therefore, we considered the possibility that other inorganic molecules play a key role in the peptide bond cleavage of Asn in vivo. However, the key molecules or ions for peptide bond cleavage are undefined. Inorganic phosphate is suggested to be related to aging because decreasing inorganic phosphate is associated with decreasing telomere length, increasing inflammatory status, and genomic DNA hypomethylation.[16] Carbonate ions are related to control of intraocular pressure and speculated to be associated with the nonenzymatic reaction in αA-crystallin and AQP0. In addition, deamidation of Asn and Gln is suggested to be catalyzed by dihydrogen phosphate and hydrogen carbonate ions.[17−19] In this study, we computationally analyzed the dihydrogen phosphate- and hydrogen carbonate-catalyzed pathways of succinimide formation for peptide bond cleavage of Asn.

## RESULTS AND DISCUSSION

To investigate the reaction mechanism and activation barrier of peptide bond cleavage, we performed quantum chemical calculations for the model compound asparaginyl glycine


https://doi.org/10.1021/acsomega.1c04821
ACS Omega 2021, 6, 30078−30084

dipeptide, capped with acetyl (Ace) and methylamino (Nme) groups on the N- and C-termini, respectively (i.e., $CH_3CO$-Asn-Gly-$NHCH_3$). To investigate the reaction pathway, the simple model compound which has a glycine residue as the ($N$ + 1) residue was employed, and the most stable complex structure was used as the initial structure. $H_2PO_4^-$ and $HCO_3^-$ ions were used as catalysts included in the calculation. Although phosphate ions exist mainly as a $HPO_4^{2-}$ ions, $H_2PO_4^-$ ions are also present at significant concentrations. The $H_2PO_4^-$ ion in particular has been proposed to serve as a catalyst for nonenzymatic post-translational modifications in several previous studies.[17−23] Carbonate ions exist mainly as $HCO_3^-$ under physiological conditions. In each catalytic reaction, we calculated the peptide bond cleavage of Asn proceeded in two steps of cyclization (*gem*-hydroxylamine formation) and C-terminal fragment release for succinimide formation (Figure 2).

**Cyclization Step.** To elucidate the reaction mechanisms for the cyclization step, the optimized geometries of the reaction complex (RC), transition state 1 (TS1), and intermediate 1 (INT1) for dihydrogen phosphate- and hydrogen carbonate-catalyzed reactions are shown in Figures 3 and 4. Because the conformation and the location of catalyst

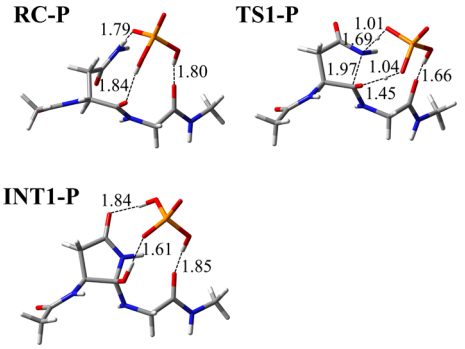


**Figure 3.** Optimized geometries of the cyclization step in dihydrogen phosphate-catalyzed reaction. The carbon, nitrogen, oxygen, and phosphorus atoms are shown in gray, blue, red, and orange, respectively. Selected interatomic distances are in units of Å.

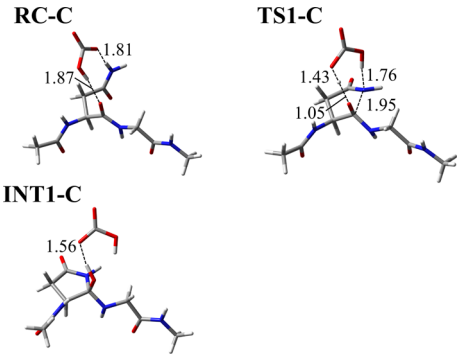


**Figure 4.** Optimized geometries of the cyclization step in the hydrogen carbonate-catalyzed reaction. The carbon, nitrogen, and oxygen atoms are shown in gray, blue, and red, respectively. Selected interatomic distances are in units of Å.

ions in intermediates were different between the cyclization and C-terminal fragment release steps, intermediates were defined as INT1 and INT2 in the cyclization and C-terminal fragment release steps, respectively. In RC, the catalysts bridged the side chain and main chain of the model compound through hydrogen bond formation. The $H_2PO_4^-$ ion formed three hydrogen bonds with the model compound: one to the hydrogen atom of the side-chain amide nitrogen of Asn, the other one to the main-chain oxygen of Asn, and another one to the main-chain oxygen of Gly. The $HCO_3^-$ ion formed two hydrogen bonds with the hydrogen atom of the side-chain amide nitrogen of Asn and the main-chain oxygen of Asn, whereas hydrogen bonds with the main-chain atoms of Gly were not observed. In TS1, all migrating hydrogen atoms are located near the catalyst ions in each reaction. The distances between the main-chain carbon and the side-chain nitrogen were 1.97 and 1.95 Å in the dihydrogen phosphate- and hydrogen carbonate-catalyzed reactions, respectively. These distances were shorter than those in deamidation, which are 2.20−2.23 and 2.01−2.24 Å in the dihydrogen phosphate- and hydrogen carbonate-catalyzed reactions, respectively.[19] In the cyclization step of peptide bond cleavage in uncatalyzed and water-catalyzed reactions, the proton transfers were almost completed.[15] On the other hand, the C−N distances forming cyclic imide in TS1 of the dihydrogen phosphate- and hydrogen carbonate-catalyzed reactions were shorter than those of uncatalyzed (2.238 Å) and water-catalyzed reactions (2.254 Å). Therefore, all proton transfers are required for the cyclization reaction in uncatalyzed and water-catalyzed reactions, while proton abstraction from amide nitrogen of the side chain is crucial for the dihydrogen phosphate- and hydrogen carbonate-catalyzed reactions. In INT1, the nucleophilic attack and the proton transfers were completed. Although only one hydrogen bond was observed in INT1-C of the hydrogen carbonate catalytic reaction, three hydrogen bonds were formed between the $H_2PO_4^-$ ion and the model compound. The hydrogen bond formed between the $H_2PO_4^-$ ion and the main-chain oxygen of Gly was formed throughout the cyclization step, and the distance of these hydrogen-bonding atoms was shortened from 1.80 Å in RC-P to 1.66 Å in TS1-P. The hydrogen bond with the main-chain oxygen of Gly is thought to stabilize the complex of the model compound and the $H_2PO_4^-$ ion. In contrast, the interaction between the $HCO_3^-$ ion and the model compound may be relatively weak. The difference in the number of hydrogen bond formation is also observed in Asn deamidation.[19] In deamidation of Asn, the $H_2PO_4^-$ ion forms with the main-chain oxygen of the ($N$ − 1) residue. The dihydrogen phosphate ions may easily bind to Asn residues to catalyze nonenzymatic reactions, in comparison with hydrogen carbonate ions. The dihedral angles of all optimized geometries in the cyclization step are shown in Table 1. The dihedral angles of the dihydrogen phosphate-catalyzed reaction were similar to those of the most stable

**Table 1. Dihedral Angles (degrees) for Asn of the Optimized Geometries for the Cyclization Step in the Dihydrogen Phosphate- and Hydrogen Carbonate-Catalyzed Reaction**

| | dihedral angle/degree | | | | | |
|---|---|---|---|---|---|---|
| | dihydrogen phosphate-catalyzed reaction | | | hydrogen carbonate-catalyzed reaction | | |
| | $\varphi$ | $\psi$ | $\chi$ | $\varphi$ | $\psi$ | $\chi$ |
| RC | −151 | 147 | −173 | −127 | 118 | −176 |
| TS1 | −142 | 98.5 | 167 | −143 | 98.6 | 164 |
| INT1 | −143 | 83.5 | 145 | −152 | 86.3 | 147 |



https://doi.org/10.1021/acsomega.1c04821
ACS Omega 2021, 6, 30078−30084

conformers of RC ($\varphi$: −156, $\psi$: 168, and $\chi$: −154) and INT ($\varphi$: −142, $\psi$: 84.8, and $\chi$: 150). The slightly conformational changes were needed to form RC. The dihedral angle $\psi$ of RC is similar to that of Asn101 in the $\alpha$A-crystallin experimental structure (139.3°) (PDB ID: 3L1F). Almost no change of dihedral angle $\varphi$ was observed in the dihydrogen phosphate-catalyzed reaction, that is, 9.1° in TS1-P formation. In the hydrogen carbonate-catalyzed reaction, the dihedral angle $\varphi$ was changed by 16° in TS1-C formation and 25° from RC-C to INT1-C. Large changes in the dihedral angle $\psi$ occurred in the dihydrogen phosphate-catalyzed reaction (48.9° in TS1-P formation), which is larger than the change of $\psi$ for Asn deamidation (31.2°) and Asp stereoinversion (38°).[19,21] On the other hand, the change of $\psi$ in the hydrogen carbonate−catalytic reaction is small (19.4°). The small change in the dihedral angle $\chi$ was observed in the cyclization step of both dihydrogen phosphate- and hydrogen carbonate-catalyzed reactions, and the change was 20° in both TS1-C and INT1-C formations. According to the computational results of $\varphi$, $\psi$, and $\chi$, the structural change of the main chain on the C-terminal side is required for the cyclization step.

**C-Terminal Fragment Release Step.** To elucidate the reaction mechanisms for the C-terminal fragment release step, the optimized geometries of intermediate 2 (INT2), transition state 2 (TS2), and product complex (PC) of dihydrogen phosphate- and hydrogen carbonate-catalyzed reactions are shown in Figures 5 and 6, respectively. INT2 is the reactant

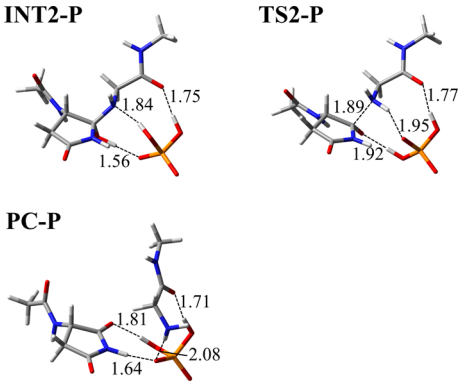


**Figure 5.** Optimized geometries of the C-terminal fragment release step in the dihydrogen phosphate-catalyzed reaction. The carbon, nitrogen, oxygen, and phosphorus atoms are shown in gray, blue, red, and orange, respectively. Selected interatomic distances are in units of Å.

complex for the C-terminal fragment release step, and locations of the catalytic ions were different from INT1. This rearrangement of the catalytic ions is thought to be energetically accessible. In INT2, catalytic ions formed the hydrogen bonds with the OH hydrogen and the nitrogen of *gem*-hydroxylamine moiety both in dihydrogen phosphate- and hydrogen carbonate-catalyzed reactions. In addition, the hydrogen bond between the $H_2PO_4^-$ ion and the main-chain oxygen of Gly was maintained. In TS2, the proton transfers were almost completed, and the C−N distances of the *gem*-hydroxylamine moiety were extended to 1.89 and 1.94 Å in the dihydrogen phosphate- and hydrogen carbonate-catalyzed reactions, respectively. These distances were similar to those in deamidation.[19] In the TS2 of water-catalyzed reactions in the peptide bond cleavage, the protons are located in the middle of the reaction associating atoms, and the C−N

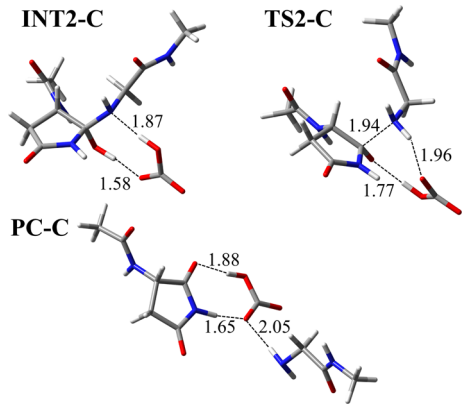


**Figure 6.** Optimized geometries of the C-terminal fragment release step in hydrogen carbonate-catalyzed reaction. The carbon, nitrogen, and oxygen atoms are shown in gray, blue, and red, respectively. Selected interatomic distances are in units of Å.

distance of *gem*-hydroxyl amine is 1.558 Å.[15] Therefore, the cleavage is considered to be coincident with the proton transfer in the water-catalyzed reaction; in contrast, the proton transfer occurred in advance of cleavage in the dihydrogen phosphate- and hydrogen carbonate-catalyzed reaction (Figures S1 and S2). The C-terminal fragment release and succinimide formation resulted in PC. The $H_2PO_4^-$ ion formed two hydrogen bonds with succinimide and two hydrogen bonds with the C-terminal fragment in PC-P. The $HCO_3^-$ ion formed two hydrogen bonds with succinimide and one hydrogen bond with the C-terminal fragment in PC-C. The hydrogen bond with the main-chain oxygen of the C-terminal fragment was not observed in the hydrogen carbonate-catalyzed reaction. The dihedral angles of all optimized geometries in the C-terminal fragment release step are shown in Table 2. Because

**Table 2. Dihedral Angles (Degrees) for Asn of the Optimized Geometries for the C-Terminal Fragment Release Step in the Dihydrogen Phosphate- and Hydrogen Carbonate-Catalyzed Reaction**

| | dihedral angle/degree | | | | | |
|---|---|---|---|---|---|---|
| | dihydrogen phosphate-catalyzed reaction | | | hydrogen carbonate-catalyzed reaction | | |
| | $\varphi$ | $\psi$ | $\chi$ | $\varphi$ | $\psi$ | $\chi$ |
| INT2 | −147 | 93.1 | 146 | −153 | 94.8 | 145 |
| TS2 | −164 | 118 | 134 | −167 | 123 | 130 |
| PC | −115 | | 138 | −117 | | 137 |

the nitrogen atom of Gly was released, the dihedral angle $\psi$ could not be evaluated in PC. The dihedral angles were similar to those of the most conformers of RC and INT without catalyst ions both in catalytic reactions. The dihedral angle $\varphi$ was changed by approximately 50° in PC formation for dihydrogen phosphate- and hydrogen carbonate-catalyzed reactions. Both $\varphi$ values were similar to that of Asn101 in the $\alpha$A-crystallin experimental structure (−112.4°). In contrast, the changes of dihedral angles $\psi$ and $\chi$ were 25−30° and 4−15°, respectively. The structural change of the main chain is not observed in the deammoniation step in Asn and Gln deamidation.[18,19] Therefore, progress of C-terminal fragment release step requires the structural change of the main chain on the N-terminal side. The dihedral angles of all optimized geometries lie in the Ramachandran plot.[24,25] In


https://doi.org/10.1021/acsomega.1c04821
ACS Omega 2021, 6, 30078−30084

particular, the dihedral angles of RC in peptide bond cleavage lie in the $\beta$-region of the Ramachandran plot. This result consists with the conformation of Asn101 in $\alpha$A-crystallin, which forms $\beta$-sheet. The dihedral angles and solvent-accessible surface area (SASA)[26] of Asn residues in crystallin experimental structures are shown in Table S1. The SASAs of Asn14, Asn37, and Asn143 of $\gamma$S-crystallin, which are frequently deamidated residues,[27] were larger than 70 Å$^2$.

Only Asn101 has >70 Å$^2$ of SASA, and the dihedral angles $\varphi$ or $\psi$ with difference less than 10° between the optimized geometries obtained in this study. This may be the reason why peptide bond cleavage is observed in Asn101 of $\alpha$A-crystallin.

**Activation Energy for Succinimide Formation of Peptide Bond Cleavage at the C-Terminal Side of Asn.** To evaluate the activation barrier for peptide bond cleavage of Asn and compare the barriers between the dihydrogen phosphate and hydrogen carbonate reactions, the energy diagram is shown in Figure 7. The relative energies were

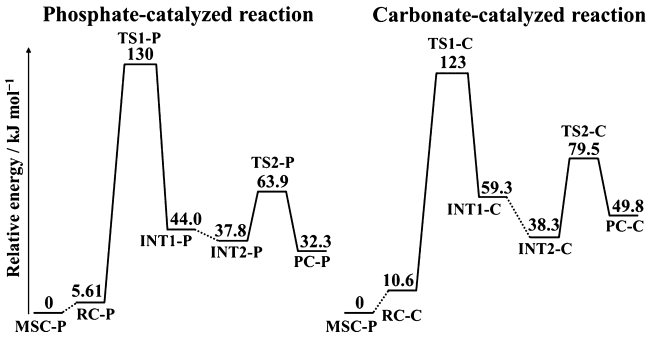


**Figure 7.** Energy profiles for the dihydrogen phosphate- and hydrogen carbonate-catalyzed peptide bond cleavage at the C-terminal side of Asn. The relative energies with respect to each most stable complex (MSC) are in units of kJ mol$^{-1}$. All energy was calculated using the MP2/6-311+G(2d,2p)//B3LYP/6-31+G(d,p) level.

calculated using the MP2/6-311+G(2d,2p)//B3LYP/6-31+G(d,p) level. In each catalyzed reaction, the rate-limiting step of peptide bond cleavage was the cyclization step because TS1 had the highest energy. The calculated activation barrier was 130 and 123 kJ mol$^{-1}$ in the dihydrogen phosphate- and hydrogen carbonate-catalyzed reactions, respectively. This result suggested that the peptide bond cleavage of Asn can proceed in the presence of $H_2PO_4^-$ or $HCO_3^-$ ions. The experimental reaction rate of peptide bond cleavage is much slower than that of deamidation, and the experimental activation barrier of Asn deamidation is 80−100 kJ mol$^{-1}$.[28,29] Therefore, the calculated activation barrier of peptide bond cleavage in this study is considered to be reasonable. In addition, the concentration of phosphate ions is higher than the concentration of carbonate ions in the cell and vice versa for the extracellular fluid.[30−32] Therefore, both ions are considered to be the major catalysts for the peptide bond cleavage of Asn, both inside and outside cells. The relative energy of PC was higher than that of RC in each catalyzed reaction because succinimide is an intermediate of the peptide bond cleavage of Asn. The succinimide intermediate is converted to Asn and isoAsn. Therefore, the peptide bond cleavage can occur in the absence of a thermodynamic driving force.

## CONCLUSIONS

In this study, we performed quantum chemical calculations to investigate the mechanism underlying the peptide bond cleavage at the C-terminal side of an Asn residue, which proceeds through cyclization and C-terminal fragment release steps. By the cyclization step, the *gem*-hydroxylamine intermediates were generated, and then, the C-terminal fragment release was led by the proton transfers. All proton transfers were mediated by the catalyst ions. The activation barriers of the dihydrogen phosphate- and hydrogen carbonate-catalyzed reactions were 130 and 123 kJ mol$^{-1}$, respectively. These values were consistent with the slow progress of the peptide bond cleavage of Asn observed in vivo. We focused on the rate-determining step and show the differences between deamidation and peptide bond cleavage in the hydrogen phosphate-catalyzed reaction (Table 3). The

**Table 3. Comparison between Deamidation and Peptide Bond Cleavage of Asn Residues**

| | deamidation | peptide bond cleavage |
|---|---|---|
| structural change of the main chain | almost remained | changes $\varphi$ and $\psi$ needed |
| C−N distance in TS1 | 2.20−2.23 Å | 1.97 Å |
| hydrogen bond formation | with N-terminal side oxygen | with C-terminal side oxygen |
| beginning the reaction | proton abstraction from amide nitrogen by the catalyst | proton abstraction from amide nitrogen by the catalyst |
| rate-determining step | cyclization step | cyclization step |

dihydrogen phosphate ion is needed to begin both reactions by proton abstraction from amide nitrogen. Differences in the dihedral angles and C−N distance in TS1 were observed.

In the hydrogen carbonate-catalyzed reaction, the change in $\psi$ was smaller than the change in the dihydrogen phosphate-catalyzed reaction. Because the $\psi$ values of TS1 were almost identical in both catalytic reactions, the difference in the change of $\psi$ in the cyclization step was due to the difference in the conformation of RC. Namely, the $\psi$ value in RC-P was closer to the value in TS1-P in the hydrogen carbonate-catalyzed reaction than that in the dihydrogen phosphate-catalyzed reaction. Therefore, the major catalyst molecules may be altered by the protein structures, such as main-chain conformation of the Asn residue. The p$K_a$ values of $H_2CO_3$, $HCO_3^-$ are 6.36 and 10.34, respectively.[33] The p$K_a$ values of $H_3PO_4$, $H_2PO_4^-$, and $HPO_4^{2-}$ are 2.14, 7.20, and 12.34, respectively. The pH of cytosol ranges from 7.0 to 7.4 and can change depending on cellular activities.[34,35] In contrast, the pH of blood ranges from 7.35 to 7.45 under normal conditions.[27] If the intracellular cell pH drops from 7.4 to 7.0, the concentration of $H_2PO_4^-$ ion will increase by 1.6-fold. Therefore, the reaction rate of the dihydrogen phosphate-catalyzed reaction in vivo may be significantly affected by changes in pH.

Our results suggest that the regulation of the concentration of $H_2PO_4^-$ or $HCO_3^-$ ions can suppress progression of age-related diseases. In addition, our results are useful for determining purification and storage methods for peptide- or protein-based drugs, including therapeutic monoclonal antibodies by better controlling fragmentation. The reaction rate of the peptide bond cleavage is affected by the species of ($N$ +


https://doi.org/10.1021/acsomega.1c04821
ACS Omega 2021, 6, 30078−30084

1) residue. When the $(N + 1)$ residue is Pro, the peptide bond cleavage is the principal degradative pathway for Asn.[2] In a future study, the effect of the side chain for the $(N + 1)$ residue on the reaction rate and mechanisms should be clarified.

## COMPUTATIONAL METHODS

The model compound used in this study was a dipeptide of asparaginyl glycine capped with acetyl (Ace) and methylamino (Nme) groups on the N- and C-termini, respectively (i.e., $CH_3CO$-Asn-Gly-$NHCH_3$). The structure of the model compound is shown in Figure 8. This figure also shows the

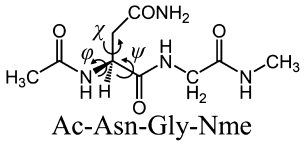


**Figure 8.** Structure of model compound structure used in this study.

dihedral angles $\varphi$ (C−N−$C_\alpha$−C) and $\psi$ (N−$C_\alpha$−C−N), which characterize the main-chain conformation, and $\chi$ (N−$C_\alpha$−$C_\beta$−C$\gamma$), which characterizes the side-chain conformation. A dihydrogen phosphate ($H_2PO_4^-$) ion and a hydrogen carbonate ion ($HCO_3^-$) were included as the catalysts in the calculations. The calculations for dihydrogen phosphate- and hydrogen carbonate-catalyzed reactions were performed several times to obtain the appropriate geometries of RC. A systematic conformational search was performed at each stationary point. To obtain stable conformers, the dihedral angles of the rotatable bonds were changed, and the structures were optimized. The optimized conformers are shown in Figures S3−S5. Furthermore, various binding modes of the catalytic ions were tested, and the most stable complex was obtained (Figures S6 and S7). All calculations were performed using Gaussian 16 software.[36] Optimization of minimum and TS geometries were performed without any constraints by density functional theory (DFT) calculations using the B3LYP exchange−correlation functional and the 6-31+G(d,p) basis set. To confirm that each TS is connected to energy-minimum geometries, intrinsic reaction coordinate (IRC) calculations were performed from TSs, followed by full geometry optimizations. We corrected the relative energies for the zero-point energy by vibrational frequency calculations for all of the optimized geometries. In addition, the single-point energies of all optimized geometries were calculated by the MP2/6-311+G(2d,2p) level. All calculations included hydration effects by employing the polarizable continuum model (PCM).

## ASSOCIATED CONTENT

### Supporting Information

The Supporting Information is available free of charge at https://pubs.acs.org/doi/10.1021/acsomega.1c04821.

Representative geometries on the IRC of the C-terminal fragment release step; dihedral angles and SASA in experimental crystallin structures; coordination of all atoms for all optimized geometries; calculated energy of all optimized geometries; and conformations obtained by conformational search (PDF)

## AUTHOR INFORMATION

### Corresponding Author

**Koichi Kato** − *Faculty of Pharmaceutical Sciences, Shonan University of Medical Sciences, Yokohama, Kanagawa 244-0806, Japan; College of Pharmacy, Kinjo Gakuin University, Nagoya, Aichi 463-8521, Japan; Faculty of Pharmacy, Meijo University, Nagoya, Aichi 468-8503, Japan;* orcid.org/0000-0001-6984-2343; Phone: +81-45-821-0111; Email: kato-k@kinjo-u.ac.jp

### Authors

**Tomoki Nakayoshi** − *Faculty of Pharmacy, Meijo University, Nagoya, Aichi 468-8503, Japan; Graduate School of Information Sciences, Hiroshima City University, Hiroshima 731-3194, Japan*

**Yoshinobu Ishikawa** − *Faculty of Pharmaceutical Sciences, Shonan University of Medical Sciences, Yokohama, Kanagawa 244-0806, Japan*

**Eiji Kurimoto** − *Faculty of Pharmacy, Meijo University, Nagoya, Aichi 468-8503, Japan*

**Akifumi Oda** − *Faculty of Pharmacy, Meijo University, Nagoya, Aichi 468-8503, Japan; Institute for Protein Research, Osaka University, Suita, Osaka 565-0871, Japan;* orcid.org/0000-0001-6487-7977

Complete contact information is available at: https://pubs.acs.org/10.1021/acsomega.1c04821

### Author Contributions

The manuscript was written through contributions of all authors. All authors have given approval to the final version of the manuscript.

### Funding

This work was supported by Grants-in-Aid for Scientific Research (17K08257, 19J23595, and 21K15244) from the Japan Society for the Promotion of Science. We are grateful to the Ministry of Education, Culture, Sports, Science and Technology (MEXT) for a Grant-in-Aid for Scientific Research on Transformative Research Areas (A) "Hyper-Ordered Structures Science" (20H05883).

### Notes

The authors declare no competing financial interest.

## REFERENCES

(1) Geiger, T.; Clarke, S. Deamidation, isomerization, and racemization at asparaginyl and aspartyl residues in peptides. Succinimide-linked reactions that contribute to protein degradation. *J. Biol. Chem.* **1987**, *262*, 785−794.

(2) Robinson, N. E.; Robinson, A. B. *Molecular Clocks: Deamidation of Asparaginyl and Glutaminyl Residues in Peptides and Proteins*; Althouse Press: Cave Junction, Oregon, 2004; pp 27−50.

(3) Capasso, S.; Mazzarella, L.; Sorrentino, G.; Balboni, G.; Kirby, A. J. Kinetics and mechanism of the cleavage of the peptide bond next to asparagine. *Peptides* **1996**, *17*, 1075−1077.

(4) Voorter, C. E.; de Haard-Hoekman, W. A.; van den Oetelaar, P. J.; Bloemendal, H.; de Jong, W. W. Spontaneous peptide bond cleavage in aging alpha-crystallin through a succinimide intermediate. *J. Biol. Chem.* **1988**, *263*, 19020−19023.

(5) Ball, L. E.; Garland, D. L.; Crouch, R. K.; Schey, K. L. Post-translational modifications of aquaporin 0 (AQP0) in the normal human lens: spatial and temporal occurrence. *Biochemistry* **2004**, *43*, 9856−9865.

(6) Palmer, W. G.; Papaconstantinou, J. Aging of -Crystallins During Development of the Lens. *Proc. Natl. Acad. Sci. U.S.A.* **1969**, *64*, 404−410.

(7) Lampi, K. J.; Wilmarth, P. A.; Murray, M. R.; David, L. L. Lens β-crystallins: The role of deamidation and related modifications in aging and cataract. *Prog. Biophys. Mol. Biol.* **2014**, *115*, 21−31.
(8) Sindhu Kumari, S.; Gupta, N.; Shiels, A.; FitzGerald, P. G.; Menon, A. G.; Mathias, R. T.; Varadaraj, K. Role of Aquaporin 0 in lens biomechanics. *Biochem. Biophys. Res. Commun.* **2015**, *462*, 339−345.
(9) Friedrich, M. G.; Wang, Z.; Schey, K. L.; Truscott, R. J. W. Mechanism of protein cleavage at asparagine leading to protein-protein cross-links. *Biochem. J.* **2019**, *476*, 3817−3834.
(10) Friedrich, M. G.; Wang, Z.; Schey, K. L.; Truscott, R. J. W. Spontaneous cross-linking of proteins at aspartate and asparagine residues is mediated via a succinimide intermediate. *Biochem. J.* **2018**, *475*, 3189−3200.
(11) Brennan, T. V.; Clarke, S. Mechanism of Cleavage at ASN 148 during the Maturation of Jack Bean Concanavalin A. *Biochem. Biophys. Res. Commun.* **1993**, *193*, 1031−1037.
(12) Gao, S. X.; Zhang, Y.; Stansberry-Perkins, K.; Buko, A.; Bai, S.; Nguyen, V.; Brader, M. L. Fragmentation of a highly purified monoclonal antibody attributed to residual CHO cell protease activity. *Biotechnol. Bioeng.* **2011**, *108*, 977−982.
(13) Vlasak, J.; Ionescu, R. Fragmentation of monoclonal antibodies. *MAbs* **2011**, *3*, 253−263.
(14) Capasso, S.; Mazzarella, L.; Kirby, A. J.; Salvadori, S. Succinimide-mediated pathway for peptide bond cleavage: Kinetic study on an Asn-Sar containing peptide. *Biopolymers* **1996**, *40*, 543−551.
(15) Catak, S.; Monard, G.; Aviyente, V.; Ruiz-López, M. F. Computational study on nonenzymatic peptide bond cleavage at asparagine and aspartic acid. *J. Phys. Chem. A* **2008**, *112*, 8752−8761.
(16) McClelland, R.; Christensen, K.; Mohammed, S.; McGuinness, D.; Cooney, J.; Bakshi, A.; Demou, E.; MacDonald, E.; Caslake, M.; Stenvinkel, P.; et al. Accelerated ageing and renal dysfunction links lower socioeconomic status and dietary phosphate intake. *Aging* **2016**, *8*, 1135−1149.
(17) Kirikoshi, R.; Manabe, N.; Takahashi, O. Succinimide formation from an NGR-containing cyclic peptide: Computational evidence for catalytic roles of phosphate buffer and the arginine side chain. *Int. J. Mol. Sci.* **2017**, *18*, 429.
(18) Kato, K.; Nakayoshi, T.; Kurimoto, E.; Oda, A. Computational studies on the nonenzymatic deamidation mechanisms of glutamine residues. *ACS Omega* **2019**, *4*, 3508−3513.
(19) Kato, K.; Nakayoshi, T.; Kurimoto, E.; Oda, A. Mechanisms of deamidation of asparagine residues and effects of main-chain conformation on activation energy. *Int. J. Mol. Sci.* **2020**, *21*, 7035.
(20) Nakayoshi, T.; Kato, K.; Fukuyoshi, S.; Takahashi, O.; Kurimoto, E.; Oda, A. Comparison of the activation energy barrier for succinimide formation from α- and β-aspartic acid residues obtained from density functional theory calculations. *Biochim. Biophys. Acta, Proteins Proteomics* **2018**, *1866*, 759−766.
(21) Kirikoshi, R.; Manabe, N.; Takahashi, O. Phosphate-catalyzed succinimide formation from asp residues: A computational study of the mechanism. *Int. J. Mol. Sci.* **2018**, *19*, 637.
(22) Nakayoshi, T.; Kato, K.; Kurimoto, E.; Oda, A. Possible mechanisms of nonenzymatic formation of dehydroalanine residue catalyzed by dihydrogen phosphate ion. *J. Phys. Chem. B* **2019**, *123*, 3147−3155.
(23) Nakayoshi, T.; Kato, K.; Kurimoto, E.; Oda, A. Computational studies on the mechanisms of nonenzymatic intramolecular cyclization of the glutamine residues located at N-termini catalyzed by inorganic phosphate Species. *ACS Omega* **2020**, *5*, 9162−9170.
(24) Ramachandran, G. N.; Sasisekharan, V. Conformation of polypeptides and proteins. *Adv. Protein Chem.* **1968**, *23*, 283−437.
(25) Kalmankar, N. V.; Ramakrishnan, C.; Balaram, P. Sparsely populated residue conformations in protein structures: revisiting "experimental" Ramachandran maps. *Proteins* **2014**, *82*, 1101−1112.
(26) Lapko, V. N.; Purkiss, A. G.; Smith, D. L.; Smith, J. B. Deamidation in Human γS-Crystallin from Cataractous Lenses Is Influenced by Surface Exposure. *Biochemistry* **2002**, *41*, 8638−8648.
(27) *PyMOL. The PyMOL Molecular Graphics System*, Version 2.0; Schrödinger, LLC, 2015.
(28) Connolly, B. D.; Tran, B.; Moore, J. M. R.; Sharma, V. K.; Kosky, A. Specific catalysis of asparaginyl deamidation by carboxylic acids: kinetic, thermodynamic, and quantitative structure-property relationship analyses. *Mol. Pharm.* **2014**, *11*, 1345−1358.
(29) Patel, K.; Borchardt, R. T. Chemical pathways of peptide degradation. II. Kinetics of deamidation of an asparaginyl residue in a model hexapeptide. *Pharm. Res.* **1990**, *07*, 703−711.
(30) Bevington, A.; Mundy, K. I.; Yates, A. J. P.; Kanis, J. A.; Russell, R. G. G.; Taylor, D. J.; Rajagopalan, B.; Radda, G. K. A study of intracellular orthophosphate concentration in human muscle and erythrocytes by 31P nuclear magnetic resonance spectroscopy and selective chemical assay. *Clin. Sci.* **1986**, *71*, 729−735.
(31) Massry, S. G.; Maschio, G.; Ritz, E. *Phosphate and Mineral Metabolism*; Plenum Press: New York, 1984; pp 463−470.
(32) Bhagavan, N. V. Water, Acids, Bases, and Buffers. *Medical Biochemistry*, 4th ed.; Harcourt/Academic Press: Massachusetts, 2002; pp 1−16.
(33) Powell, K. J.; Brown, P. L.; Byrne, R. H.; Gajda, T.; Hefter, G.; Sjöberg, S.; Wanner, H. Chemical speciation of environmentally significant heavy metals with inorganic ligands. Part 1: The Hg2+- Cl-, OH-, CO32-, SO42-, and PO43- aqueous systems (IUPAC Technical Report). *Pure Appl. Chem.* **2005**, *77*, 739−800.
(34) Roos, A.; Boron, W. F. Intracellular pH. *Physiol. Rev.* **1981**, *61*, 296−434.
(35) Madshus, I. H. Regulation of intracellular pH in eukaryotic cells. *Biochem. J.* **1988**, *250*, 1−8.
(36) Frisch, M. J.; Trucks, G. W.; Schlegel, H. B.; Scuseria, G. E.; Robb, M. A.; Cheeseman, J. R.; Scalmani, G.; Barone, V.; Petersson, G. A.; Nakatsuji, H.; et al. *Gaussian 16*, Revision A.03; Gaussian Inc.: Wallingford CT, 2016.


https://doi.org/10.1021/acsomega.1c04821
*ACS Omega* 2021, 6, 30078−30084